ACSNANO
www.acsnano.org
ARTICLE

Microfluidic Diffusion Analysis of the Sizes and Interactions of Proteins under Native Solution Conditions

Paolo Arosio,[†,§] Thomas Müller,[†,‡,§] Luke Rajah,[†,§] Emma V. Yates,[†] Francesco A. Aprile,[†] Yingbo Zhang,[†] Samuel I. A. Cohen,[†] Duncan A. White,[†] Therese W. Herling,[†] Erwin J. De Genst,[†] Sara Linse,[¶] Michele Vendruscolo,[†] Christopher M. Dobson,[†] and Tuomas P. J. Knowles*[,†]

[†]Department of Chemistry, University of Cambridge, Lensfield Road, Cambridge CB2 1EW, U.K.
[‡]Fluidic Analytics Ltd., Cambridge CB2 1EW, U.K.
[¶]Department of Biochemistry and Structural Biology, Lund University, Box 124, SE221 00 Lund, Sweden

Supporting Information

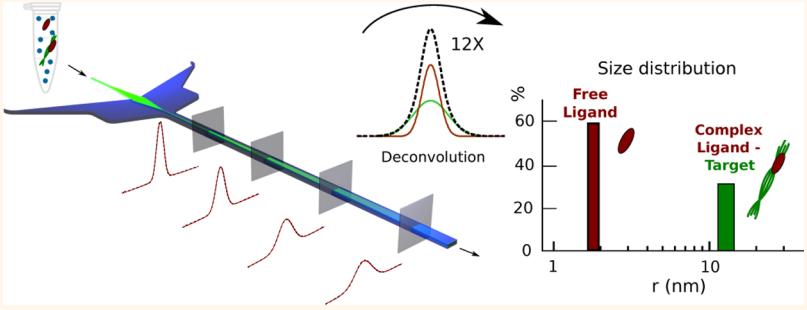

ABSTRACT: **Characterizing the sizes and interactions of macromolecules under native conditions is a challenging problem in many areas of molecular sciences, which fundamentally arises from the polydisperse nature of biomolecular mixtures. Here, we describe a microfluidic platform for diffusional sizing based on monitoring micron-scale mass transport simultaneously in space and time. We show that the global analysis of such combined space−time data enables the hydrodynamic radii of individual species within mixtures to be determined directly by deconvoluting average signals into the contributions from the individual species. We demonstrate that the ability to perform rapid noninvasive sizing allows this method to be used to characterize interactions between biomolecules under native conditions. We illustrate the potential of the technique by implementing a single-step quantitative immunoassay that operates on a time scale of seconds and detects specific interactions between biomolecules within complex mixtures.**

KEYWORDS: *size distribution, interactions, proteins, diffusion, polydispersity, immunoassay*

Many systems of both fundamental and technological importance are characterized by the presence of polydisperse mixtures of heterogeneous components. In particular, the majority of proteins fulfill their biological roles not as monomeric species but as components of larger functional complexes.[1,2] The characterization of such complexes has important implications in biological and medical sciences, both for understanding normal functional behavior and because aberrant interactions between molecules can lead to dysfunction and disease.[3−5]

The diffusivity of macromolecules and colloids in solution is a fundamental physicochemical property and represents a powerful probe of their sizes and structures. Diffusion coefficients can be determined in free solution, are sensitive reporters of biomolecular binding, and do not require the presence of matrices or attachment to surfaces for their measurement. As a result, a range of experimental techniques have been developed to measure the diffusion coefficients of macromolecules in solution. Conventional approaches to such measurements include nuclear magnetic resonance (NMR) spectroscopy,[6,7] dynamic light scattering (DLS),[8,9] and fluorescence correlation spectroscopy (FCS).[10−12] More recently, techniques to monitor diffusion behavior in microfluidic channels have also been proposed.[13−19] All these methods typically rely on monitoring the evolution of a signal, for example, resonance, scattering, or fluorescence efficiency, generated by an object either in time or in space. Such evolution is directly related to the diffusive motion of

Received: July 29, 2015
Accepted: December 17, 2015
Published: December 17, 2015

DOI: 10.1021/acsnano.5b04713
ACS Nano 2016, 10, 333−341

the object, and the measurement of the signal allows the quantification of its diffusion coefficient.[8,10] An important alternative technique to diffusion-based approaches to evaluate the size and structure of macromolecules in solution is analytical ultracentrifugation, which separates components on the basis of their sedimentation coefficients.[20−22] All these approaches are able to determine the size of species in the nanometer to micron range and perform best when applied to pure homogeneous samples.

Evaluating the properties of polydisperse mixtures in solution is, however, extremely challenging with the currently available biophysical techniques since the evaluation of the complete size distribution of the component species requires the deconvolution of an average signal, which is a very difficult inverse problem,[9] although sophisticated mathematical approaches have been developed that can to some extent address this limitation.[23,24] An additional challenge is that many sizing techniques are susceptible to systematic biases; in dynamic light scattering, for example, the average value of the hydrodynamic radius of mixtures is dominated by the larger species in the sample because of the strong dependence of the scattering intensity on the particle radius, as described by the Rayleigh formalism.[8] This problem is conventionally addressed by physically separating the individual components within a mixture, for instance, by gel filtration or another chromatographic method, and detecting and sizing the individual fractionated species, for example, by absorbance or light scattering.[25,26] This approach poses its own challenges, however, as the separation procedure may modify the distribution of sizes, for example, because of the interaction of one or more of the components with the separation medium or by the need for long analysis times or a significant dilution of the sample.[27]

To overcome the problem of measuring polydisperse samples and to probe mixtures of components or their interactions, attractive approaches have been developed, which project the species into the gas phase to enable mass spectrometric techniques to be used. A variety of methods have been developed to mantain native-like properties correlating with those in solution and then to evaluate the mobility of individual species in the gas phase using time-of-flight techniques and applying electric fields.[28−31] Such methods have proved to be very powerful, but experiments can be challenging to optimize in order to minimize any differences between the gas and solution phases and the changes in the balance of interactions in the different media.

In this work, we propose a fundamentaly different approach to measure the diffusion coefficients of specific species directly in solution by tracking simultaneously the spatial and the temporal evolution of their diffusion. We show that the acquisition of the diffusion profiles in two dimensions—space and time—increases the information content with respect to single profiles acquired in either space or time, and that such two-dimensional diffusion profiles can be modeled by diffusive and advection mass transport equations, resulting in the determination of accurate diffusion coefficients by rigorous interpretation of the experimental data without the need for any *a priori* knowledge of the analyte composition. We have implemented the concept of a single-step two-dimensional approach on a microfluidic platform, which offers a series of advantages over conventional techniques, including significant reductions in the amounts of sample and time that are required for the analysis as well as in the degree to which analytes interact with surfaces.[32,33]

RESULTS AND DISCUSSION

Monitoring Diffusion in Space and Time on a Microfluidic Platform. We have developed an approach that allows the determination of diffusion profiles resulting from the Brownian motion of analyte particles initially localized in a well-defined region of space. Measurements were performed simultaneously for multiple diffusion times as the analyte spreads through diffusion, and the diffusion times were selected in order to capture the different time scales over which the smallest and the largest particles in the analyte solution diffuse over the same length scale. We have implemented this concept in a microfluidic device fabricated using soft lithography methods.[34] Schematic diagrams and a picture of the device are shown in Figure 1a−c (see also Figure S1). Measurements were conducted by flow-focusing an analyte stream in the middle of the channel between

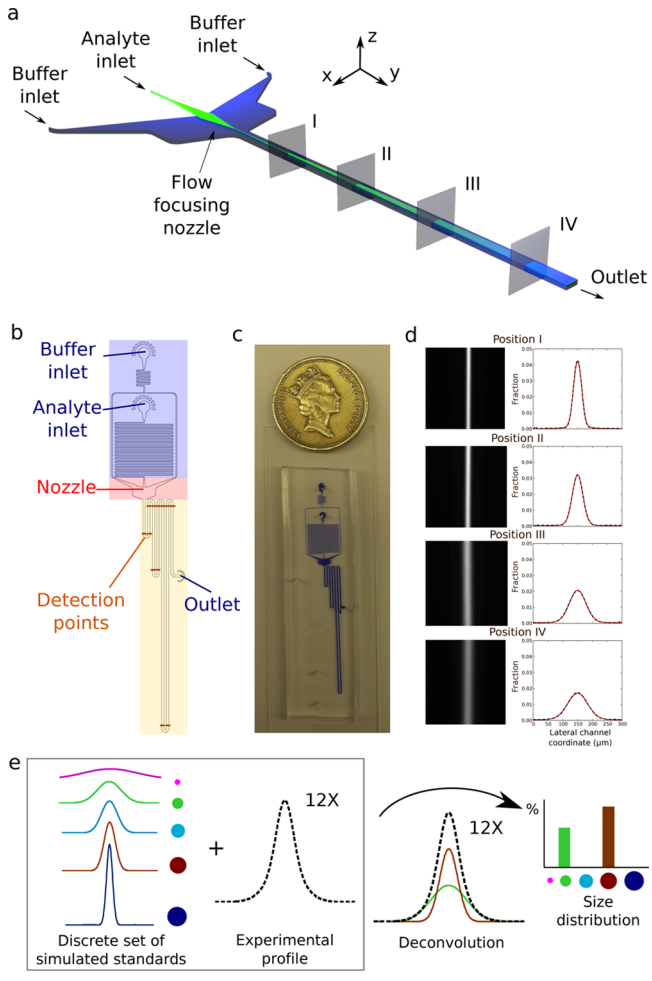

Figure 1. Microfluidic space−time diffusion device. (a,b) Design of the device highlighting its most relevant components. (c) Picture of the device, where the channels have been filled with a Coomassie blue solution to make them visible. (d) Experimental images of diffused fluorescent colloid analytes at different positions (corresponding to different diffusion times) along the channel and comparison between the corresponding measured (dotted black lines) and simulated (continuous red lines) diffusion profiles. (e) Global analysis of several diffusion profiles acquired in both time and space enables the deconvolution of the experimental signal into a linear combination of simulated standard profiles, thereby leading to the evaluation of the size distribution of the components of the mixture.

DOI: 10.1021/acsnano.5b04713
ACS Nano 2016, 10, 333−341

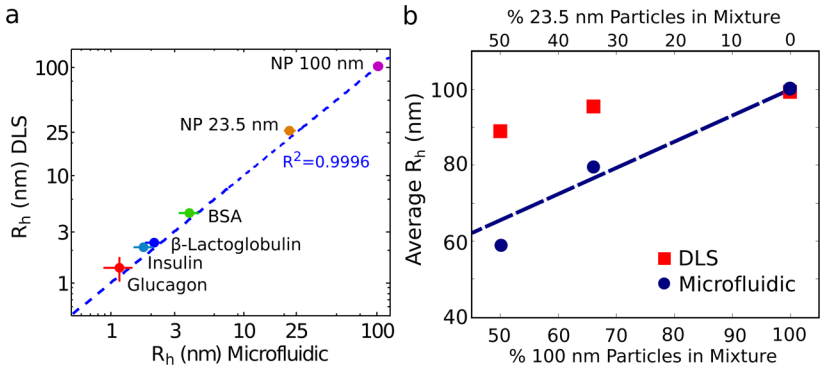

Figure 2. Average sizes of the components of monodisperse and polydisperse solutions. Average hydrodynamic radii of monodisperse solutions of several proteins and standard nanoparticles (NPs) (a) and of binary mixtures of 23.5 and 100 nm NPs with different ratios of the two components (b), as measured by the microfluidic device and by conventional dynamic light scattering. The dashed line in (a) represents a fit to the equation $y = x$, and the dashed line in (b) represents the expected average size of the colloid mixtures.

two streams of an auxiliary fluid and observing the diffusive spreading of the components of the analyte solution as they travel downstream along the channel. In this device, the analyte and the auxiliary fluid are loaded into inlet reservoirs, and the solution flow rate is controlled by applying a negative pressure at the device outlet with a syringe pump.

A crucial requirement for the quantitative interpretation of the results is the accurate positioning of the analyte in a well-defined initial configuration before any diffusion is allowed to take place. In order to minimize undesirable diffusion prior to the measurements, we developed a multistage nozzle to allow the analyte and buffer solution to merge in a channel 10 times wider than the channel in which diffusion is to be monitored.[35] Once this well-defined initial spatial localization of the analyte molecules has been generated, the diffusive spreading is measured in the device at multiple (typically 12) points along the channel, each corresponding to a different diffusion time. In this work, the diffusion profiles are recorded through epi-fluorescence microscopy (see Methods), which allows high sensitive detection of proteins at concentrations as low as a few nM. Figure 1d shows typical microscopy images of a test sample of fluorescent colloids at different positions along the channel. The requirement for fluorescence microscopy is, however, not inherent to our approach since the detection can occur by alternative concentration-dependent methods, such as UV absorption. A high channel aspect ratio of 1:12 has been chosen to ensure a high Péclet number in the x-direction and a low Péclet number in the z-direction, such that all particles explore the full height of the channel during their residence time within the device.[15,36]

One key feature of this method is that the typical residence time in the channel, during which diffusion occurs, is on the order of 15−60 s, significantly shorter than the times required for conventional diffusion or chromatography-based approaches. These short time scales make this approach particularly attractive for measuring the size distribution of complexes in rapid and dynamic equilibrium. The residence time can be selected in order to guarantee sufficient diffusive transport in the channel to provide information on the diffusivity and, at the same time, to avoid the analyte diffusing all the way to the side of the channel, at which point information on diffusive motion is lost.

This measurement procedure can be carried out under a wide range of solution conditions, allowing proteins to be studied in their native states. Moreover, unlike with many other solution-state sizing techniques, such as capillary electrophoresis, Taylor dispersion, single-particle tracking, and other proposed microfluidic diffusion techniques,[17] measurements are performed under steady-state flow, thereby allowing the investigation of samples at lower concentrations with respect to other methods that do not operate under steady-state conditions, simply by increasing the detection time.

Measurements of Monodisperse and Polydisperse Solutions. We first validated the microfluidic space−time diffusion device by comparing the hydrodynamic radii (R_H) of a series of monodisperse species measured by this approach with the values obtained by conventional DLS techniques. A set of peptides, proteins, and fluorescent polymer nanoparticles covering a wide range of sizes from 1 to 100 nm was selected. The peptides and proteins were labeled before the analysis with the latent fluorophore *o*-phthalaldehyde (OPA)[19] (see Methods). Since the free dye is not fluorescent within our detection limit, no purification steps are required prior to the analysis.[19]

The flow in the channel takes place at low Reynolds numbers (in the range of 0.07−0.6), where inertial forces can be neglected relative to viscous forces, and advection and diffusion are the only relevant mechanisms of mass transport.[37] The diffusion coefficient D of a given analyte is determined by comparing the experimental measurements of mass transport with the numerical solution to the diffusion−advection equation (see online methods), without requiring calibration against known standards. The diffusion coefficient informs directly on the hydrodynamic radius $R_H = kT/6\pi\eta D$ of the analyte (Figure 1e). Here, T is the temperature and η is the solvent viscosity.

The hydrodynamic radii of the proteins shown in Figure 2 have been measured in solutions containing 20%v/v dimethyl sulfoxide (DMSO); such denaturing conditions ensure the presence of a monodisperse monomeric state and to allow definitive comparison with light scattering techniques. We will then move on to measurements under native conditions to study protein−protein interactions in the absence of denaturants. Figure 2a demonstrates the excellent agreement between the two approaches for homogeneous solutions, revealing the reliability of the microfluidic assay developed in this work (see also Table S1); the average deviation in R_H for different repeats of the same sample is around 15%. Note that the measurements using the microfluidic technique require a significantly lower amount of analyte with respect to DLS, in particular, for species with sizes equal to or smaller than a few nanometers, for which concentrations 1 order of magnitude higher with respect to the microfluidic technique are needed to generate a detectable

DOI: 10.1021/acsnano.5b04713
ACS Nano 2016, 10, 333−341

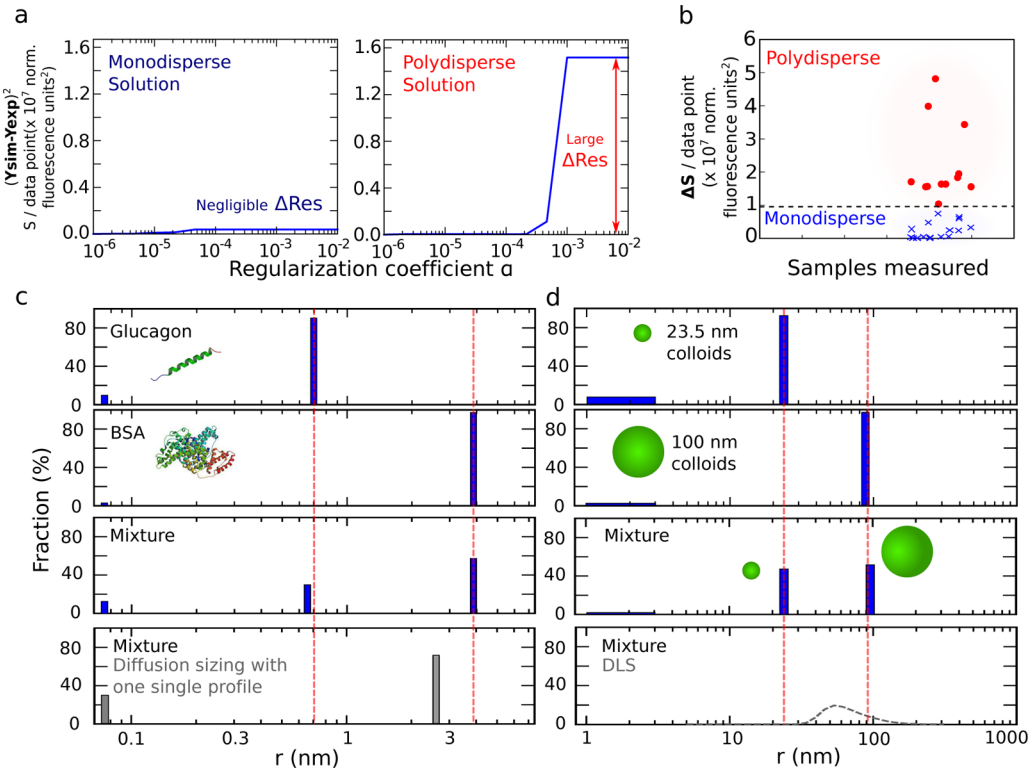

Figure 3. Polydispersity and size distributions. (a) Changes in the sum of squared residuals, *S*, per data point (in normalized fluorescence units squared) upon increase of the regularization coefficient α for a monodisperse solution (glucagon) and a polydisperse solution (a 1:1 mixture of glucagon and BSA). In the limit of very high penalty coefficients α, the size distribution is represented by a single peak. In this regime, a large error is therefore introduced when attempting to describe polydisperse solutions. (b) Difference in the sum of squared residuals between experimental and simulated data obtained with $\alpha = 10^{-6}$ and $\alpha = 10^{-2}$ using various monodisperse solutions (blue crosses) as well as binary and ternary mixtures (red circles) of nanoparticles and amino acids/proteins/peptides, namely, tyrosine, glucagon, β-lactoglobulin, insulin, and BSA. The dashed line represents the threshold between monodisperse and polydisperse solutions. (c,d) Sizing of binary mixtures of proteins (c) and of nanocolloids of different diameters (d): the radii of the individual species measured in the mixture are very close to those evaluated in the homogeneous solutions. The acquisition of a single diffusion profile, which is typical in conventional diffusion sizing approaches such as dynamic light scattering, is not sufficient here to resolve the binary distribution (gray bars in panel (c)). The gray dotted line in (d) represents the size distribution measured by dynamic light scattering, which under these conditions does not resolve the two component peaks.

scattering signal using DLS. In addition, with the present method we measured successfully particles with hydrodynamic diameters up to 500 nm, indicating that the microfluidic technique exhibits a dynamic range comparable to DLS. Another advantage of our approach compared to conventional DLS is the absence of a bias toward larger species[9] when the average size of heterogeneous mixtures is evaluated, as shown in Figure 2b, where the average hydrodynamic radii of mixtures of nanoparticles with 23.5 and 100 nm diameters are reported. We observe that DLS measurements commonly overestimate the average size of the mixtures.

We next demonstrated the power of the microfluidic space–time diffusion technique for analyzing mixtures of proteins and nanoparticles. The acquisition of multiple diffusion profiles at different diffusion times is the key development that allows the deconvolution of the profiles into the contributions of the discrete species. The shape of the concentration profile $c(x)$ contains information about the complete distribution of the diffusion coefficients $\rho(D_i)$ of the species present in solution as a linear superposition, such that $c(x) = \sum_i \rho_i B_y(r_i,x)$, where the kernel $B_y(r_i,x)$ describes the distribution perpendicular to the channel length of a species with a given hydrodynamic radius r_i at location y along the channel.[23] To obtain the distribution of coefficients $\rho(D_i)$ as a function of their diffusion coefficients, we inverted the linear superposition relationship using a regularization algorithm to ensure stability even in the presence of experimental noise. Specifically, our strategy consists of increasing progressively the number of species starting from one single component ($N = 1$, $N = 2$, $N = 3$, ...), and evaluating whether or not the addition of a species improves the description of the experimental data within the observed noise level. We implement this concept by introducing a regularization coefficient, α, which is determined by calibration with known standards, as described in the following (see also Figure S2). This analysis does not introduce any bias toward either smaller or larger species because of the linear dependence of the signal on the concentration of the individual components.

Figure 3a shows the changes in the sum of squared residuals, *S*, upon increase of the regularization coefficient α for a monodisperse solution (pure glucagon) and for a polydisperse solution (an approximately 1:1 mixture of glucagon and bovine serum albumin (BSA)). The flow rate in experiments and simulated basis functions was 160 μL/h, and all experiments were performed in a 20 mM phosphate buffer solution at pH 8.0 containing 20%v/v DMSO to prevent intermolecular interactions between the proteins in the mixture, which may lead to association events or modification of the pure thermal diffusion motion of the species. In the limit of very high regularization coefficients α, the size distribution is represented by a single peak, and in this regime, a large error is therefore introduced when

DOI: 10.1021/acsnano.5b04713
ACS Nano 2016, 10, 333–341

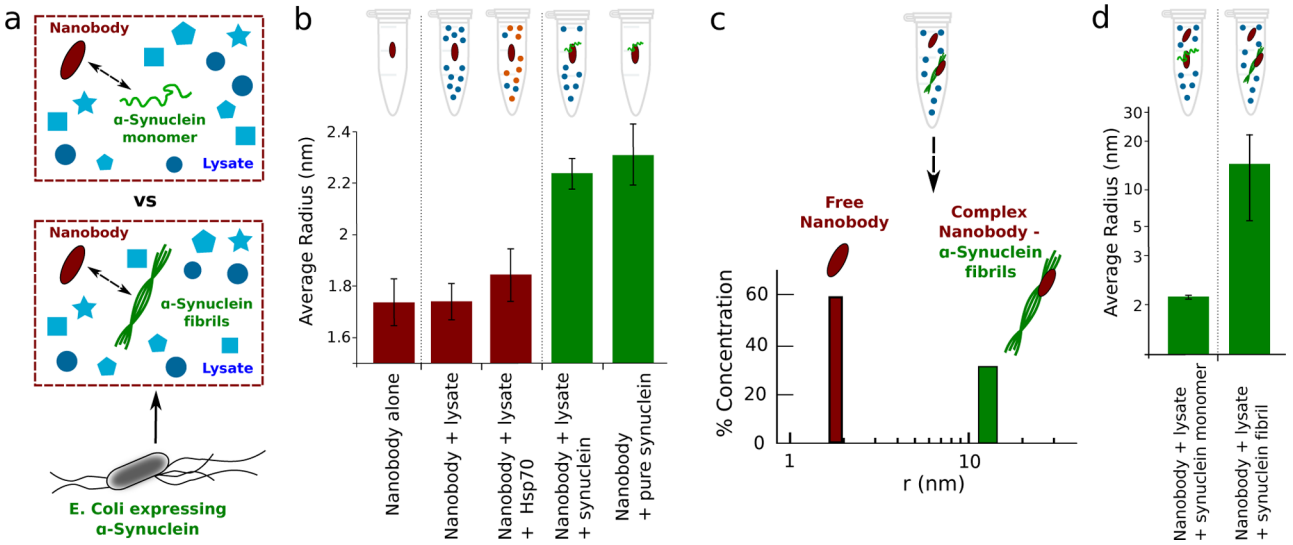

Figure 4. Detection of specific interactions and identification of protein conformation in a heterogeneous mixture: (a) schematic of the system, showing the specific binding of a labeled nanobody to α-synuclein in a cell lysate. (b) Change in size of the nanobody in the presence of α-synuclein allows the detection of the binding not only in the homogeneous solution but also in the mixture, where many other proteins are present. Negative controls, represented by lysates where either no protein or a protein that does not interact with the nanobody (in this case the molecular chaperone Hsp70) has been overexpressed, are also shown. (c) Size distribution of a mixture represented by the nanobody and α-synuclein fibrils added into a cell lysate in which monomeric α-synuclein had not been expressed. (d) Absolute measurement of the hydrodynamic radius allows not only the detection of the presence of the target species but also the identification of the conformation of the species in the lysate.

attempting to describe polydisperse solutions; by contrast, monodisperse solutions are much less sensitive to the regularization procedure since they are by their very nature well-described by a single size. We can exploit this situation to distinguish between polydisperse and monodisperse solutions by evaluating the difference in the sum of squared residuals between experimental data and simulations obtained with $\alpha = 10^{-6}$ (corresponding to a negligible penalty for many species) and $\alpha = 10^{-2}$, where only a single species is allowed in the distribution. In Figure 3b, we report this difference in squared residuals for various monodisperse solutions as well as binary and ternary mixtures of nanoparticles and of amino acids, peptides, and proteins, namely, tyrosine, glucagon, β-lactoglobulin, insulin, and BSA. We note that for all monodisperse samples the change in the sum of squared residuals lies below 10^{-7} normalized fluorescence units squared per data point, which can therefore be defined as the empirical limit between apparently monodisperse and polydisperse solutions.

This behavior is further illustrated in Figure 3c,d, where we show the size distributions of monodisperse solutions of glucagon and BSA and of nanoparticles with radii of 23.5 and 100 nm, as well as the size distributions of mixtures of two components. The technique is able to resolve the sizes of the two individual species in the mixture, providing values which are equal to the radii measured in the corresponding homogeneous solutions (see also Figure S2). For comparison, in Figure 3d, we also report the size distribution of the same mixture measured by DLS, which under these conditions is not able to resolve the two different populations due to the dominance of the scattering of the larger particles. We emphasize that the acquisition of a large number of diffusion profiles (in this work, this number was fixed to be 12) is a key factor in increasing the robustness of the global fitting procedure against random and systematic experimental error, therefore allowing the clear resolution of the individual peaks of a binary mixture (see also Figure S3). When only a single diffusion profile is considered in the fitting procedure, by analogy with the situation observed to occur in conventional diffusional sizing approaches, such as DLS or NMR, it is typically challenging to resolve readily individual peaks corresponding to the components of a binary mixture (Figure 3c), demonstrating the importance of the multidimensional data acquisition strategy.

In order to evaluate the limits of the technique in resolving polydispersity, we forced simulated binary mixtures of particles with one fixed radius $r_1 = 3.7$ nm and one variable radius r_2 (from 0.74 to 18.5 nm) to be represented by a single species and calculated the increase in the sum of squared residuals per data point (in normalized fluorescence units squared) of the fits with one single component with respect to the corresponding fits with two species (see Figure S4). In order to ensure fitting to just a single size, the regularization coefficient α was set to be 10^{-2}, and the basis functions for the simulations were computed using a flow rate of 160 μL/h. Comparison of Figure S4 with Figure 3b indicates that the sizes of two individual species must differ by about a factor 3 in order to be resolved, and indeed, experiments performed with binary mixtures of species having different ratios of sizes between the two components show that resolution of the individual components without any *a priori* knowledge of the system is possible only where this ratio exceeds the threshold value of $r_2/r_1 = 3$ (see Figure S4).

In summary, the analysis of the changes in residuals as a function of the regularization coefficient α (Figure 3a,b) allows us to determine whether an unknown sample is monodisperse or polydisperse (within our resolution limit of a factor of 3 in size between components). For monodisperse samples, the size of the single component is measured by considering the largest value of the parameter α in the analysis. If the sample is polydisperse, the technique can identify the principal components within the mixture which differ of a factor of 3 in size. In this case, the analysis has to be performed by considering the

DOI: 10.1021/acsnano.5b04713
ACS Nano 2016, 10, 333−341

smallest coefficient α that corresponds to a size distribution with the minimal number of components differing by a factor of 3 in size (see also Figure S2).

Detecting Specific Interactions between Biomolecules in a Complex Mixture. The microfluidic diffusion approach developed here has a wide variety of potential applications in the field of colloidal and biological systems. One of the many relevant examples is the investigation of interactions between proteins and nanoparticles in biological fluids.[38,39] Of particular interest is the opportunity to probe specific interactions between biomolecules in a heterogeneous multicomponent mixture, a problem that is ubiquitous in the biological sciences. Some of the most powerful of the currently available methodologies to address this challenge are immunoassays, including Western blotting, but such approaches require the fractionation of samples followed by staining with primary and secondary antibodies. Other methods, such as ELISA, require the immobilization of samples on a surface, a procedure that can lead to background signals and perturbation of the interactions. Moreover, additional procedures required by some of these methods, such as, for example, washing steps, could prevent the detection of transient interactions. In this section, we show how the microfluidic platform described in the present paper allows the direct detection of specific target species within a complex mixture in a quantitative manner, under native conditions, without the need for purification or for immobilization on a surface.

We illustrate this application by probing the binding between α-synuclein, a protein whose aggregation is associated with the development of Parkinson's disease, and a single domain antibody fragment (denoted as a nanobody) NbSyn87[38,39] inside a crude cell lysate that has been prepared from cells expressing α-synuclein but that also contains a heterogeneous population of other cellular proteins. The nanobody was labeled prior to addition to the lysate with Alexa Fluor 647 to allow detection by fluorescence methods, but no processing of the crude cell lysate was carried out. The formation of a complex between α-synuclein and the nanobody will give rise to an increase in the hydrodynamic radius relative to the individual components, the detection of which would confirm the presence of a specific interaction. As negative controls, we examined crude lysates in which α-synuclein had not been expressed, and, as a positive control, we monitored the binding between the nanobody and α-synuclein in a purified homogeneous preparation.

Figure 4a shows a schematic illustration of these experiments, and SDS-PAGE analysis of the samples is reported in Figure S5. The results show that the microfluidic technique is indeed able to detect the increase in the apparent size of the nanobody upon binding to monomeric α-synuclein in the purified homogeneous solution, with R_H changing from 1.77 ± 0.06 to 2.31 ± 0.11 nm, reflecting the slower diffusion of the labeled nanobody when incorporated into the complex. Crucially, the same result was observed when the binding experiments were carried out in the cell lysates, with R_H changing from 1.77 ± 0.06 to 2.24 ± 0.06 nm (Figure 4b). In the negative controls, using cell lysates from *Escherichia coli* strains which do not overexpress α-synuclein, the hydrodynamic radius of the fluorescent species was observed to be that of the nanobody alone, confirming the absence of interactions between the nanobody and any other proteins in the lysate.

A key feature of this technique is that it is not limited to the binary detection of the presence of the target species, as the measurement of hydrodynamic radius also allows the identification of the conformation of the species in the lysate, which, in the case of α-synuclein, for example, may involve either monomeric or aggregated forms of the protein. We demonstrate this concept by using the microfluidic immunoassay to define the size distribution of a mixture of the nanobody and α-synuclein fibrils added into in a cell lysate in which monomeric α-synuclein had not been expressed. The results show a bimodal size disitribution (Figure 4c), with one species observed to have a hydrodynamic radius of *ca.* 1.8 nm, which is equivalent to the R_H of the free nanobody in solution (Figure 4b), and a second species with a much larger R_H in the range from 11 to 60 nm, which can be associated with the complex resulting from the interactions between the nanobody and α-synuclein fibrils; this nanobody binds to the fibrils as well as the monomeric species because the epitope is located at the C-terminus of synuclein that is not incorporated into the aggregated species.[38,39] The fact that the hydrodynamic radius of this complex with the fibrils is much larger than the value of the assembly formed by the nanobody and monomeric α-synuclein (Figure 4d) demonstrates that the measurement of the R_H allows not only the qualitative detection of the target species but also the identification of its conformation.

In addition, the evaluation of size makes the microfluidic space−time method a quantitative tool for the measurement of titration curves and thereby of the dissociation constant K_d as well as of the stoichiometry of the complex. In Figure S6, we show an example of this application by plotting the increase in the average radius at increasing concentrations of α-synuclein at a fixed concentration of nanobody, indicating the formation of the complex when the concentration of the substrate exceeds the K_d.

CONCLUSIONS

In summary, we have demonstrated a microfluidic diffusion technique that is able to monitor quantitatively the diffusion of specific molecules in both space and time. The basis of this technique is the multidimensional acquisition of diffusion profiles at different diffusion times, which represents a fundamentally new development that allows high sizing resolution to be achieved by generating multiple contraints in the fitting of simulated diffusion profiles to experimental data, independently of the detection method. This approach allows the estimation of diffusion coefficients with high accuracy, thus enabling the definition of the average sizes and polydispersity of homogeneous and heterogeneous solutions. The method as implemented here is able to resolve the hydrodynamic radii of individual components within binary mixtures differing in size of a factor of 3, thereby making it possible to monitor many bimolecular interactions by tracking the time evolution of bimodal size distributions.

We have illustrated the potential of this approach with a microfluidic immunoassay that can detect specific interactions between biomolecules in complex mixtures, allowing the identification of the presence and of the configuration of target species in heterogeneous solutions. In addition, the evaluation of the size allows the measurement of titration curves, and thereby of the dissociation constant K_d as well as of the stoichiometry of the complex. Besides being applicable to heterogeneous systems, the technique monitors species under steady-state conditions, is carried out in the solution state, and requires sample volumes of as little as a few microliters. In addition, the rapid analysis time (on the order of seconds) and the limited requirement for analyte dilution make this approach attractive for the sizing of complexes

DOI: 10.1021/acsnano.5b04713
ACS Nano 2016, 10, 333−341

in rapid dynamic equilibrium and for the detection of interactions directly in solution and under native conditions. We believe, therefore, that this technique will have a multitude of potential applications in the determination of the sizes and interactions of a wide range of biomolecules within native-like environments.

METHODS

Materials. Green fluorescent polystyrene nanoparticles with nominal diameters of 47 or 200 nm and density of 1.06 kg/dm^3 were supplied by ThermoFisher Scientific (Waltham, MA, USA). Excitation and emission maxima are 468 and 508 nm, respectively. All amino acids and proteins were purchased from Sigma-Aldrich (St. Louis, MO, USA), expect for human wt α-synuclein (gi:80475099), which was recombinantly expressed and purified from *E. coli* BL21 (DE3) gold (Stratagene) as described previously.[40] Both pure α-synuclein and α-synuclein in the crude extract were used in the binding experiments. Crude cell extracts from cells expressing either no protein or recombinant N-hexa-His-tagged Hsp70 (Hsp70 1A, gi:194248072)[41] were produced in a similar way to extracts expressing human wt α-synuclein. The final total concentration of proteins in the crude lysates, evaluated by UV absorbance, was about 800 μM, and the amount of α-synuclein, estimated from the intensities of the bands in SDS-PAGE gels, was about 16% of the total protein load.

The antibody fragment, NbSyn87, was previously isolated through phage display selection following the immunization of a llama with the A53T variant of human α-synuclein,[39] and the expression and purification of NbSyn87 was performed according to the protocol described in the same paper.[39] To obtain Alexa Fluor 647 labeled NbSyn87, we mixed a solution of 70 nmol of NbSyn87 with 1.5 equiv of Alexa Fluor 647-succinimidyl ester (Life Technologies, Paisley, UK) in 1 mL of 100 mM sodium carbonate buffer at pH 9.0. The reaction mixture was incubated in the dark at room temperature for 5 h, and subsequently, the free dye was separated from the labeled protein using PD10 desalting columns, containing 8.3 mL of Sephadex G-25 resin (GE-Healthcare, Little Chalfont, UK). The labeling yield and stoichiometry were determined spectrophotometrically according to the manufacturer's recommendations.

Fabrication of the Microfluidic Device and Details of Its Use. Microfluidic channels were fabricated by standard soft-lithography techniques[34] casting polydimethylsiloxane (PDMS) (Sylgard 184 kit; Dow Corning, Midland, MI, USA) on a master wafer, curing it at 65 °C for 75 min, peeling it off, and bonding it to a glass slide after plasma activation. The channel height was 25 μm. The channel width was 300 μm in the detection region, 3000 μm at the nozzle, and 100 μm in the hydrodynamic resistors introducing buffer and analyte into the nozzle. The flow in the channel was controlled by applying negative pressure at the outlet by using a syringe pump (Cetoni neMESYS, Cetoni GmbH, Korbussen, Germany) at flow rates in the range of 40−320 μL/h. Such flow rates correspond to a residence time in the channel of 7.5−60 s and a Reynolds number of 0.07−0.6. The diffusion times were selected in order to capture the different time scales over which the smallest and the largest particles in the analyte solution diffuse over the same length scale. The analyte and the buffer were loaded into the corresponding reservoirs located at the inlets. A single measurement typically required 10 μL of sample.

The solutions were illuminated using a LED light source (Cairn Research, Faversham, UK) equipped with suitable filter sets (Chroma Technology Corporation, Bellows Falls, VT, USA) for the specific fluorophore. In particular, the range of excitation and emission wavelengths were 450−490 and 500−550 nm (49002 ET-EGFP) for the green nanoparticles, 325−375 and 433−485 nm (49000 ET-DAPI) for the OPA-labeled proteins, as well as 624−654 and 668−718 nm (49009 ET-Cy5) for the nanobody labeled with Alexa Fluor 647, respectively. Images were collected at 12 different points along the channel at downstream distances between 10 and 100 mm using an inverted microscope (Axio Observer D1, Zeiss, Cambridge, UK) equipped with a fluorescent illumination system (OptoLED, Cairn Research, Faversham, UK) and a cooled CCD camera (Evolve 512, Photometrics, Tucson, AZ, USA). Typical exposure times were in the range of 3−10 s.

Labeling of Protein Solutions. Peptide and protein solutions were prepared at a concentration of 1 g/L in 20 mM phosphate buffer at pH 8.0 with 20%v/v DMSO. The protein solutions were labeled with the latent fluorophore OPA that in the presence of β-mercaptoethanol (BME) reacts with primary amines exposed on the surface of the proteins to form a bicyclic, isoindole-type fluorophore *in situ*.[42] Since the unreacted dye is not fluorescent, this labeling technique does not require any purification steps before the analysis. Protein sizes have been measured under denaturing conditions to guarantee the presence of a monodisperse monomeric state and to allow reliable comparison with light scattering. Stock solutions with 60 mM OPA and 90 mM BME were freshly prepared in 20 mM phosphate buffer at pH 8.0. The reagents were introduced into the protein solutions at a final concentration of OPA and BME of 1 and 1.5 mM, respectively, to ensure that the quantities of these reagents were in each case comparable to the concentration of primary amines in the system (of about 1 mM). After addition of the reagents, the protein solutions were incubated at room temperature for 1 h before starting the measurements.

Measurements of Monodisperse and Polydisperse Solutions. Nanoparticle dispersions in distilled water at a volume fraction of 0.05% were used for the diffusion measurements. Suitable mixtures were prepared by mixing homogeneous dispersions of the two components. Homogeneous protein solutions were prepared at concentrations of 1 g/L, and the heterogeneous mixtures were prepared by mixing the corresponding homogeneous solutions at suitable ratios to provide comparable amounts of primary amines for the different proteins, thus ensuring that each component would give rise to a comparable fluorescent signal.

Quantitative Immunoassay Based on the Specific Interactions between the Nanobody and α-Synuclein. Aliquots of the original crude mixtures containing 800 μM of total protein were diluted 10-fold into nanobody solutions of 1 μM concentration in 20 mM Tris buffer at pH 7.4 and incubated at room temperature for 1 h before starting the measurements. The concentrations of α-synuclein for the titration studies were in the range 5−25 μM.

Dynamic Light Scattering. DLS measurements were performed on a Zetasizer Nano instrument (Malvern Instruments, Malvern, UK) working in backscattering mode at 173°, equipped with a light source with a wavelength of 633 nm. Protein solutions at 10 g/L were filtered with a 20 nm cutoff filter (Anotop Filters, Whatman, Maidstone, UK) immediately before the measurements. Standard nanoparticle dispersions were measured under the same conditions in the microfluidic experiments but without filtration.

Numerical Simulation of Mass Transport under Steady-State Flow and Fitting Procedure. The mass transport under steady-state flow was simulated numerically using an approach described in detail previously.[37] Briefly, we used a particle-based approach to solve the diffusion and convection equation by propagating a large number of particles introduced at a starting point at a single fixed time. We exploited this approach to simulate a discrete set of concentration profiles, $B(r_i,x)$, for particles of a given size r_i in the microfluidic channel. The measured diffusion profiles $c(x)$ of the analyte at different diffusion times were described as linear combinations of the profiles of the simulated library. Specifically, we employed a basin hopping algorithm[43] implemented in Python performing 250 random displacements. In order to obtain the simplest solution within error, we used a regularization expressing the target function as

$$\min_{\{\rho_i\}}\left(\sum_j (c(x_j) - \sum_i \rho_i B(r_i, x_j))^2 - \alpha \sum_i \rho_i \log \rho_i\right) \quad (1)$$

where ρ_i is the linear coefficient of each simulated profile $B(r_i)$ with radius r_i, $c(x_j)$ is the measured concentration at each lateral and longitudinal channel position y_j, and α is a proportionality constant for the regularization. Similarly to other regularization methods, such as entropy maximization[23,44] or Tikhonov regularization,[45] the residuals of the fit to the experimental data are additionally penalized according to the distribution $\{\rho_i\}$. The optimal value of the parameter α was

DOI: 10.1021/acsnano.5b04713
ACS Nano 2016, 10, 333−341

determined as described in the main text (see also Figures 3 and S2). We note that the analysis could be carried out equally by directly forcing the simulated distribution to be composed of a discrete number of components (*e.g.*, $N = 1$, $N = 2$, or $N = 3$) and comparing the resulting residuals in order to determine the number of components, N, which best describes the experimental data within the noise level (see also Figure S7).

Due to the diffusion that already occurs inside the microfluidic nozzle, the experimental initial distribution was generally slightly wider than the simulated hat function. This difference could occasionally lead to a nonzero coefficient at the smallest simulated radius, and to avoid this problem the coefficient of the smallest simulated radius was excluded from the regularization.

The quality of the experimental fits were assessed by recording the sum of squared residuals per data point—not including the regularization term. Using normalized units where the total concentration in each individual experimental profile adds up to one, we typically obtained squared residuals of the order of 10^{-7} per data point. In the same units, the magnitude of the experimental noise was estimated by recording the standard deviation of the outermost ten data points at position 1 (where no analyte had yet diffused). This procedure yields an experimental noise power of the order of 10^{-8} at the concentrations of proteins used in this work. This estimation of the noise, however, only gives a lower bound for the experimental error because it does not take into account shot noise of the CCD camera at higher signals and systematic deviations such as inhomogeneities in the illumination.

ASSOCIATED CONTENT

Supporting Information

The Supporting Information is available free of charge on the ACS Publications website at DOI: 10.1021/acsnano.5b04713.

Additional material on the experimental setup, on the fitting procedure and on the resolution of the device. Comparison between the sizes of several proteins and standard nanoparticles as measured by the microfluidic device and by conventional dynamic light scattering. SDS-PAGE analysis of the samples considered in the immunobinding assay. Titration curve of the binding between the nanobody and α-synuclein (PDF)

AUTHOR INFORMATION

Corresponding Author

*E-mail: tpjk2@cam.ac.uk.

Author Contributions

§P.A., T.M., and L.R. contributed equally.

Notes

The authors declare the following competing financial interest(s): Part of the work described in this paper has been the subject of a patent application filed by Cambridge Enterprise, a wholly owned subsidiary of the University of Cambridge. This patent has been licensed to Fluidic Analytics Ltd., where T.P.J.K. is Chief Scientific Officer and member of the Board of Directors and C.M.D is a Scientific Advisor.

ACKNOWLEDGMENTS

We acknowledge financial support from the Swiss National Science Foundation (P.A., T.M.), the Marie Curie Fellowship scheme for career development (P.A.), the BBSRC (T.M., T.W.H., T.P.J.K.), the ERC (T.P.J.K.), the Frances and Augustus Newman Foundation (T.P.J.K.), and the Wellcome Trust (C.M.D., T.P.J.K.).

REFERENCES

(1) Levy, E. D.; Boeri Erba, E.; Robinson, C. V.; Teichmann, S. A. Assembly Reflects Evolution of Protein Complexes. *Nature* **2008**, *453*, 1262−1265.

(2) Robinson, C. V.; Sali, A.; Baumeister, W. The Molecular Sociology of the Cell. *Nature* **2007**, *450*, 973−982.

(3) Knowles, T. P. J.; Vendruscolo, M.; Dobson, C. M. The Amyloid State and its Association with Protein Misfolding Diseases. *Nat. Rev. Mol. Cell Biol.* **2014**, *15*, 384−396.

(4) Aguzzi, A.; O'Connor, T. Protein Aggregation Diseases: Pathogenicity and Therapeutic Perspectives. *Nat. Rev. Drug Discovery* **2010**, *9*, 237−248.

(5) Eisenberg, D.; Jucker, M. The Amyloid State of Proteins in Human Diseases. *Cell* **2012**, *148*, 1188−203.

(6) Price, W. S. Pulsed-Field Gradient Nuclear Magnetic Resonance as a Tool for Studying Translational Diffusion: Part 1. Basic Theory. *Concepts Magn. Reson.* **1997**, *9*, 299−336.

(7) Wilkins, D. K.; Grimshaw, S. B.; Receveur, V.; Dobson, C. M.; Jones, J. A.; Smith, L. J. Hydrodynamic Radii of Native and Denatured Proteins Measured by Pulse Field Gradient NMR. *Biochemistry* **1999**, *38*, 16424−16431.

(8) Berne, B.; Pecora, R. *Dynamic Light Scattering: With Applications to Chemistry, Biology, and Physics*; Wiley: New York, 2000.

(9) Lomakin, A.; Benedek, G. B.; Teplow, D. B. Monitoring Protein Assembly Using Quasielastic Light Scattering Spectroscopy. *Methods Enzymol.* **1999**, *309*, 429−459.

(10) Elson, E. L.; Magde, D. Fluorescence Correlation Spectroscopy. 1. Conceptual Basis and Theory. *Biopolymers* **1974**, *13*, 1−27.

(11) Chakraborty, M.; Kuriata, A. M.; Henderson, J. N.; Salvucci, M. E.; Wachter, R. M.; Levitus, M. Protein Oligomerization Monitored by Fluorescence Fluctuation Spectroscopy: Self-Assembly of Rubisco Activase. *Biophys. J.* **2012**, *103*, 949−958.

(12) Sengupta, P.; Garai, K.; Balaji, J.; Periasamy, N.; Maiti, S. Measuring Size Distribution in Highly Heterogeneous Systems with Fluorescence Correlation Spectroscopy. *Biophys. J.* **2003**, *84*, 1977−1984.

(13) Hatch, A.; Kamholz, A. E.; Hawkins, K. R.; Munson, M. S.; Schilling, E. A.; Weigl, B. H.; Yager, P. A Rapid Diffusion Immunoassay in a T-Sensor. *Nat. Biotechnol.* **2001**, *19*, 461−465.

(14) Hatch, A.; Garcia, E.; Yager, P. Diffusion-based Analysis of Molecular Interactions in Microfluidic Devices. *Proc. IEEE* **2004**, *92*, 126−139.

(15) Kamholz, A. E.; Schilling, E. A.; Yager, P. Optical Measurement of Transverse Molecular Diffusion in a Microchannel. *Biophys. J.* **2001**, *80*, 1967−1972.

(16) Kamholz, A. E.; Yager, P. Theoretical Analysis of Molecular Diffusion in Pressure-driven Laminar Flow in Microfluidic Channels. *Biophys. J.* **2001**, *80*, 155−160.

(17) Culbertson, C. T.; Jacobson, S.; Ramsey, J. M. Diffusion Coefficient Measurements in Microfluidic Devices. *Talanta* **2002**, *56*, 365−373.

(18) Cottet, H.; Biron, J. P.; Martin, M. Taylor Dispersion Analysis of Mixtures. *Anal. Chem.* **2007**, *79*, 9066−9073.

(19) Yates, E. V.; Mueller, T.; Rajah, L.; De Genst, E.; Arosio, P.; Linse, S. S.; Vendruscolo, M.; Dobson, C. M.; Knowles, T. P. J. Latent Analysis of Unmodified Biomolecules and their Complexes in Solution with Attomole Detection Sensitivity. *Nat. Chem.* **2015**, *7*, 802−809.

(20) Howlett, G. J.; Minton, A. P.; Rivas, G. Analytical Ultracentrifugation for the Study of Protein Association and Assembly. *Curr. Opin. Chem. Biol.* **2006**, *10*, 430−436.

(21) Lebowitz, J.; Lewis, M. S.; Schuck, P. Modern Analytical Ultracentrifugation in Protein Science: A Tutorial Review. *Protein Sci.* **2002**, *11*, 2067−2079.

(22) Rivas, G.; Stafford, W.; Minton, A. P. Characterization of Heterologous Protein-Protein Interactions Using Analytical Ultracentrifugation. *Methods* **1999**, *19*, 194−212.

(23) Schuck, P. Size-Distribution Analysis of Macromolecules by Sedimentation Velocity Ultracentrifugation and Lamm Equation Modeling. *Biophys. J.* **2000**, *78*, 1606−1619.

DOI: 10.1021/acsnano.5b04713
ACS Nano 2016, 10, 333−341

(24) Brown, P. H.; Balbo, A.; Schuck, P. A Bayesian Approach for Quantifying Trace Amounts of Antibody Aggregates by Sedimentation Velocity Analytical Ultracentrifugation. *AAPS J.* **2008**, *10*, 481−493.
(25) Kendrick, B. S.; Kerwin, B. A.; Chang, B. S.; Philo, J. S. Online Size-exclusion High-performance Liquid Chromatography Light Scattering and Differential Refractometry Methods to Determine Degree of Polymer Conjugation to Proteins and Protein-Protein or Protein-Ligand Association States. *Anal. Biochem.* **2001**, *299*, 136−146.
(26) Arosio, P.; Barolo, G.; Mueller-Spaeth, T.; Wu, H.; Morbidelli, M. Aggregation Stability of a Monoclonal Antibody During Downstream Processing. *Pharm. Res.* **2011**, *28*, 1884−1894.
(27) Carpenter, J. F.; Randolph, T. W.; Jiskoot, W.; Crommelin, D. J.; Middaugh, C. R.; Winter, G. Potential Inaccurate Quantitation and Sizing of Protein Aggregates by Size Exclusion Chromatography: Essential Need to use Orthogonal Methods to Assure the Quality of Therapeutic Protein Products. *J. Pharm. Sci.* **2010**, *99*, 2200−8.
(28) Benjamin, D. R.; Robinson, C. V.; Hendrick, J. P.; Hartl, F. U.; Dobson, C. M. Mass Spectrometry of Ribosomes and Ribosomal Subunits. *Proc. Natl. Acad. Sci. U. S. A.* **1998**, *95*, 7391−7395.
(29) Ruotolo, B. T.; Benesch, J. L. P.; Sandercock, A. M.; Hyung, S. J.; Robinson, C. V. Ion Mobility-Mass Spectrometry Analysis of Large Protein Complexes. *Nat. Protoc.* **2008**, *3*, 1139−1152.
(30) Benesch, J. L. P.; Aquilina, J. A.; Ruotolo, B. T.; Sobott, F.; Robinson, C. V. Tandem Mass Spectrometry Reveals the Quaternary Organization of Macromolecular Assemblies. *Chem. Biol.* **2006**, *13*, 597−605.
(31) Ho, Y.; Gruhler, A.; Heilbut, A.; Bader, G. D.; Moore, L.; Adams, S. L.; Millar, A.; Taylor, P.; Bennett, K.; Boutilier, K.; et al. Systematic Identification of Protein Complexes in Saccharomyces Cerevisiae by Mass Spectrometry. *Nature* **2002**, *415*, 180−183.
(32) Whitesides, G. M. The Origins and the Future of Microfluidics. *Nature* **2006**, *442*, 368−373.
(33) Cho, S.; Kang, D.-K.; Choo, J.; deMello, A. J.; Chang, S.-I. Recent Advances in Microfluidic Technologies for Biochemistry and Molecular Biology. *BMB Rep.* **2011**, *44*, 705−712.
(34) Duffy, D. C.; McDonald, J. C.; Schueller, O. J. A.; Whitesides, G. M. Rapid Prototyping of Microfluidic Systems in Poly-(dimethylsiloxane). *Anal. Chem.* **1998**, *70*, 4974−4984.
(35) Cohen, S. I. A.; Knowles, T. P. J.; Dobson, C. M.; Rajah, L.; White, D. PCT Application No. WO2014064438 A1, 2014.
(36) Ismagilov, R. F.; Stroock, A. D.; Kenis, P. J. A.; Whitesides, G. Experimental and Theoretical Scaling Laws for Transverse Diffusive Broadening in Two-phase Laminar Flows in Microchannels. *Appl. Phys. Lett.* **2000**, *76*, 2376−2378.
(37) Müllller, T.; Arosio, P.; Rajah, L.; Cohen, S. I. A.; Yates, E. V.; Vendruscolo, M.; Dobson, C. M.; Knowles, T. P. J. Simulating Steady-state Mass Transport under Flow from Velocity-weighted Particle Trajectories. *arXiv:1510.05126v1* **2015**.
(38) DeGenst, E. J.; Guilliams, T.; Wellens, J.; O'Day, E. M.; Waudby, C. A.; Meehan, S.; Dumoulin, M.; Hsu, S. D.; Cremades, N.; Verschueren, K. H. G.; et al. Structure and Properties of a Complex of alpha-Synuclein and a Single-Domain Camelid Antibody. *J. Mol. Biol.* **2010**, *402*, 326−343.
(39) Guilliams, T.; El-Turk, F.; Buell, A. K.; O'Day, E. M.; Aprile, F. A.; Esbjörner, E.; Vendruscolo, M.; Cremades, N.; Pardon, E.; Wyns, L.; et al. Nanobodies Raised Against Monomeric Alpha-synuclein Distinguish between Fibrils at Different Maturation Stages. *J. Mol. Biol.* **2013**, *425*, 2397−411.
(40) Hoyer, W.; Antony, T.; Cherny, D.; Heim, G.; Jovin, T. M.; Subramaniam, V. Dependence of Alpha-synuclein Aggregate Morphology on Solution Conditions. *J. Mol. Biol.* **2002**, *322*, 383−393.
(41) Aprile, F. A.; Dhulesia, A.; Stengel, F.; Roodveldt, C.; Benesch, J. L. P.; Tortora, P.; Robinson, C. V.; Salvatella, X.; Dobson, C. M.; Cremades, N. Hsp70 Oligomerization Is Mediated by an Interaction between the Interdomain Linker and the Substrate-Binding Domain. *PLoS One* **2013**, *8*, 383−393.
(42) Roth, M. Fluorescence Reaction for Amino acids. *Anal. Chem.* **1971**, *43*, 880−882.
(43) Wales, D. J.; Doye, J. P. K. Global Optimization by Basin-Hopping and the Lowest Energy Structures of Lennard-Jones Clusters Containing up to 110 Atoms. *J. Phys. Chem. A* **1997**, *101*, 5111.
(44) Smith, C. R.; Grandy, J. W. T. In *Maximum-Entropy and Bayesian Methods in Inverse Problems*; Reidel, T. N., Ed.; D. Reidel: Dordrecht, The Netherlands, 1985.
(45) Phillips, D. L. A. Technique for the Numerical Solution of Certain Integral Equations of the First Kind. *J. Assoc. Comput. Mach.* **1962**, *9*, 84−97.

DOI: 10.1021/acsnano.5b04713
ACS Nano 2016, 10, 333−341